

Circulation regime fluctuations and their effect on intraseasonal variability in the ECHAM climate model

By MICHAEL PONATER*^{2,1}, WINFRIED KÖNIG¹, ROBERT SAUSEN^{2,1} and FRANK SIELMANN¹, ¹*Meteorologisches Institut der Universität Hamburg, Bundesstr. 55, D-20146 Hamburg, Germany;* ²*Institut für Physik der Atmosphäre, DLR Oberpfaffenhofen, D-82234 Wessling, Germany*

(Manuscript received 1 February 1993; in final form 26 October 1993)

ABSTRACT

The interannual variability of the observed extratropical atmosphere is known to be arranged in well-defined spatial patterns (teleconnection patterns). The representation of these patterns in multi-year runs with the ECHAM2/T21 general circulation model is investigated for Northern Hemisphere winter, applying the techniques of teleconnectivity analysis and EOF-analysis. Simulations either including or neglecting the forcing effect of interannual sea surface temperature variability (SST) are considered. Prominent modes of interannual atmospheric variability like the Atlantic oscillation, the West Pacific pattern, and the Pacific/North American pattern are all reproduced by the model. If interannual SST variations are included, the simulation of the patterns is far more realistic. The features of the Atlantic Oscillation appear to be particularly sensitive in this respect. The fluctuations of the interannual variability patterns (or regimes) have a substantial influence on the strength and the spatial structure of intraseasonal transient activity, both on the cyclonic and the low-frequency (weekly) time scale. This is consistently pointed out by conventional transient eddy statistics and by consideration of individual synoptic events. The simulated relationship between interannual variability and intraseasonal variability compares favourably with observational evidence. Hence, the results suggest that methods of deducing local climate changes from large-scale response patterns of the model may be successful.

1. Introduction

The spectral general circulation model ECHAM, and particularly its low-resolution (T21) version, is destined to serve as the atmospheric part of a coupled climate model. A number of climate change experiments have already been run with the coupled model, among which are transient CO₂-scenario experiments lasting up to 100 years (Cubasch et al., 1992). However, the three-dimensional atmospheric response developing in those long-term runs can only be accepted with confidence, if the atmospheric model is sufficiently free from systematic errors: Not only with respect to its time-mean state but also with respect to the large

scale features of low-frequency variability. Thus it is desirable to perform, under present-day climate conditions, short range experiments that can be subject to validation with observed data.

In this paper, we will focus our attention on the representation of Northern Hemisphere extratropical interannual variability patterns, as they show up in a 19-year seasonal cycle integration with the GCM version ECHAM2. The atmospheric model was run in the uncoupled mode, but to allow a fair comparison with the observed interannual variability the boundary condition was specified using 19 different annual cycles of nearly global sea surface temperature (SST) anomaly (taken from the period 1970 to 1988). This integration will be called the “GAGO”-run throughout this paper, where the technical term GAGO means “Global atmosphere-global ocean”. Similar runs

* Corresponding author.

have been investigated by Lau and Nath (1990) and by Barnett et al. (1991). The former operational T21-AGCM used by the Hamburg large-scale modelling group (Fischer, 1987; Fischer, 1989; also used by Barnett et al., 1991) displayed a rather weak level of extratropical interannual variability. Thus considerable modifications have been implemented that should favour increased low-frequency activity (together with reducing the systematic errors of the time-mean state) in the ECHAM model. These modifications include a new cloud and radiation scheme (leading to an intensification of the hydrological cycle and a more active tropical atmosphere), a new land surface parameterization (avoiding the prescription of deep soil conditions according to climatology), and a more appropriate parameterization of horizontal diffusion (intensifying the interaction of eddies of different scales in the extratropics). The ECHAM model and the basic features of the simulated time-mean state are described in detail by Roeckner et al. (1992). The discussion in the present paper will be restricted to Northern Hemisphere winter conditions, for which the observed evidence of interannual variability patterns has been most extensively documented in literature. Fig. 1 shows the long-term winter (Dec., Jan., Feb.) mean and the related interannual standard deviation for observed and simulated monthly mean 500 hPa geopotential height. The observational results were calculated from ten years of ECMWF level III b analyses (1979 to 1988). It is evident that a realistic level of extratropical interannual variability is simulated by the GAGO run performed with the ECHAM2 model. The regions of maximum variance are also correctly located. Hence it appears that the time has come for an attempt to verify the characteristic patterns of interannual variability, their temporal development, and their dependence on the specification of boundary conditions.

We will start with a brief review of the present knowledge about those patterns in the observed atmosphere (Section 2). In Section 3, we will present the results of a teleconnectivity analysis and an eigenvector analysis to demonstrate the ability of the model to reproduce the observed phenomena. In Section 4, the impact of interannual SST variability on the dynamic patterns will be pointed out by a comparison of the GAGO results with those of a "control type" 20-year

integration without interannual variability of the SST forcing. Section 5 will deal with the features of intraseasonal transient activity associated with the modes of the interannual variability patterns. A concluding discussion will be given in Section 6.

2. Observational evidence of low-frequency variability patterns

There is ample evidence that the temporal variability (on periods larger than about 30 days) of the Northern Hemisphere extratropical atmosphere during winter can be viewed as being organized in a number of well-defined spatial patterns. Each of them covers a considerable part of the hemisphere and consists of 2 to 4 centres, which are strongly correlated or anti-correlated among each other. The regions of maximum variance (Fig. 1), the "centres of action", turn out to be correlation centres of these so-called teleconnection patterns. The time evolution of different teleconnection patterns occurs to a large extent independently.

The most important points of observational studies concerning this matter shall be mentioned here (for a comprehensive review, see Kushnir and Wallace, 1989). The five dominant patterns of wintertime monthly averaged 500 mb height variability were established by Wallace and Gutzler (1981, hereafter cited as WG). They used one-point correlation maps to identify their patterns and displayed the essence of their results in the so-called "teleconnectivity map". Here, each grid point is characterized by its teleconnectivity strength, i.e., the highest negative correlation with any of the remote points. Those grid points that are related most strongly to one another in the explained way form the centres of the teleconnection patterns. Centres belonging to the same pattern are connected by arrows (see WG, their Fig. 7b, or Wallace and Blackmon, 1983, their Fig. 3.4).

The teleconnectivity concept is clearly a very simple approach. Its results are closely related to the space/time structure of the original data, thus allowing a straightforward interpretation. Its main shortcoming is the inability to appropriately separate spatially overlapping patterns. Trying to avoid this problem more sophisticated techniques have been applied. Conventional principal component analysis on the hemispheric scale proved to

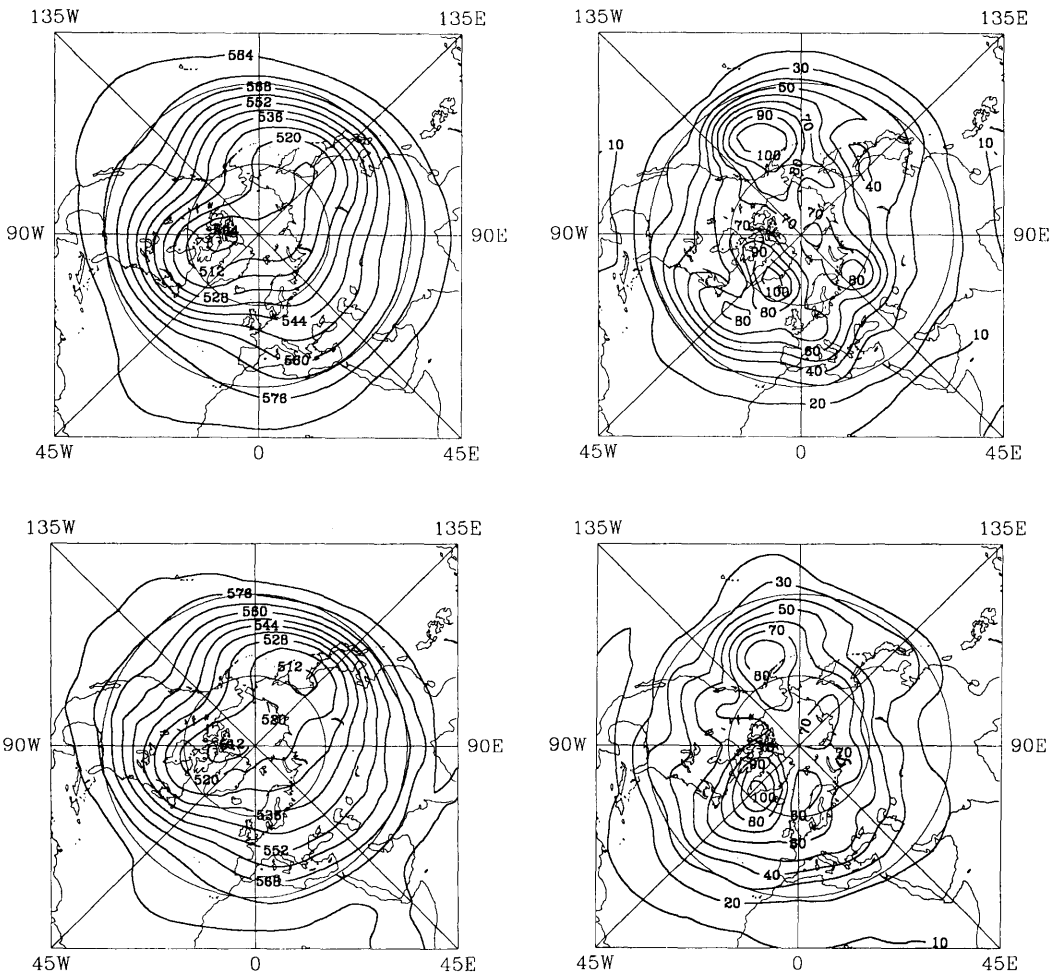


Fig. 1. Left panel shows long-term winter mean of 500 hPa geopotential height for the Northern Hemisphere (units: gpdam), top ECMWF observations, bottom ECHAM2 simulation. Right panel shows the respective interannual standard deviation of winter (Dec., Jan., Feb.) monthly means (units: gpm).

have little skill in reproducing the regional character of the teleconnection patterns. However, if the spatial patterns are rotated under certain constraints, robust structures of localized nature can be re-established. Rotated principal component analysis was used by Barnston and Livezey (1987) for a systematic investigation of interannual 700 hPa height variability. While the existence of the fundamental structures found by WG was mainly confirmed, Barnston and Livezey were able to increase the number of quasi-independent patterns by interpreting the spatial loading

vectors of higher principal components (with smaller but non-neglectable contribution to the total variance).

Refinements of the analysis were also introduced with respect to the time-scales involved. Esbensen (1984) pointed out that spectral pre-filtering of the basic time series (before calculating the correlation patterns) provides evidence of significant differences between teleconnection patterns associated with either the intraseasonal time scale or the interannual time scale. Combination of spectral filtering and rotated principal component analysis

yields well-defined, robust structures. It has been tried to demonstrate that these patterns may exhibit quite different dynamical characteristics and different energy exchange with the mean flow (Kushnir and Wallace, 1989).

3. Simulated low-frequency variability patterns

3.1. Data and data processing

Low-resolution GCMs do not represent the real world in all aspects, hence not all the subtleties of the observed patterns can be expected to be inherent in our model data. The validation of the major patterns, however, appears to be a promising task. Restricting our intentions in this respect we decided to choose the simplest and most straightforward approach. The analysis of the simulated low-frequency variability patterns was performed on the basis of monthly means of 500 hPa geopotential height fields for December, January, and February of the GAGO integration described in the introduction. The mean annual cycle was reduced by subtracting the long-term average from the individual monthly means for each calendar month. A linear trend reduction was applied. Then the fields of December, January, and February were pooled, yielding a total of 57 wintertime monthly means. According to experience, stable patterns can be expected from statistical analysis of such a magnitude of samples. However, the potential difference of intraseasonal and interannual time scale must remain hidden by this construction of the ensemble.

The data were then subjected to the teleconnectivity analysis (according to WG) and to an empirical orthogonal function analysis on a regional scale. The point-to-point correlations basic to the teleconnectivity map were calculated for the northern hemispheric part of the Gaussian transform grid associated with the T21-model. To assess the statistical significance of the resulting correlations an univariate confidence estimate can be derived from the number of degrees of freedom in the time domain. This number is not exactly known. It is surely less than the number of samples (monthly means) due to the fact that months belonging to the same season cannot be regarded as independent. However, the number of degrees of freedom should have at least a value of 18, related

to the 19 seasons entering the ensemble. Statistical significance on the 5%-level would then be indicated by a critical correlation value of 0.46. As it turns out this value is exceeded at the majority of extratropical grid points. Thus we use the reproducibility of a correlation structure (rather than statistical significance) as an indicator of its robustness. The reproducibility can be tested by repeating the analysis for sub-ensembles, for example that consisting of 19 January monthly means. While not all the complementary results can be presented here, we conclude that correlation values higher than 0.6 can be regarded to define robust correlation patterns.

For the EOF analysis, the quasi-regular Gaussian grid could not be used. The data were interpolated to a grid consisting of equal area boxes before determining the eigenvalues and eigenvectors.

3.2. Teleconnectivity analysis results

Fig. 2 shows the teleconnectivity map resulting from the GAGO simulated data. Three dominant patterns can clearly be identified and all of them have their counterparts in the real world (again see Fig. 3.4 of Wallace and Blackmon, 1983). Hence, we decided to adopt well established terms like the "Pacific/North American (PNA) pattern", the "West Pacific (WP) pattern", and the "Atlantic Oscillation" for the simulated structures. The

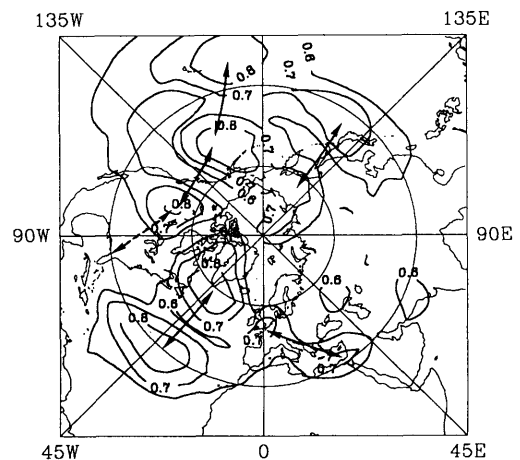


Fig. 2. Teleconnectivity map of simulated monthly mean 500 hPa geopotential height for the Northern Hemisphere in winter. The correlation centres of the dominating patterns are connected by arrows.

centres of teleconnectivity associated with the PNA-pattern are very similarly located for model and observations. These centres coincide with regions of enhanced variance (Fig. 1d) including the primary maximum south of the Aleutians. The centre over the southeastern United States is more weakly linked to the rest of the pattern than observations would require. The two separate dipole structures found by WG over the North Atlantic the "West Atlantic pattern" and the "East Atlantic pattern" cannot be distinguished for the simulation. They are represented by one single dipole (Fig. 2) with its centres being located along 40°W longitude, to the south at 30°N, and to the north at 60°N. The northern correlation maximum (over southern Greenland) coincides with the hemisphere variability maximum (Fig. 1d). The respective pattern will be referred to as the "Atlantic Oscillation" (AO) throughout this paper. Barnston and Livezey (1987) used the designation "North Atlantic Oscillation" (NAO) for a quite similar correlation structure. However, to prevent confusion with the surface pressure pattern found by Walker and Bliss (1932), a different name appears to be more appropriate. The features of the simulated WP pattern are also in reasonable agreement with their observed counterparts. (Observational evidence, e.g., Barnston and Livezey, 1987, suggests that this pattern is less robust than the structures discussed so far.). The teleconnectivity values associated with WP are weaker than for PNA and AO, but strong enough to distinguish a clear-defined pattern from the background continuum. WG and others have provided evidence of the existence of an "Eurasian pattern", though this one does not reach the same amount of correlation among its centres than the other patterns do. In the simulation, there is little to identify such a structure. Correlation coefficients over Asia do not exceed 0.6 in general and the teleconnectivity map is almost featureless in that part of the hemisphere.

It can be summarized that the GAGO simulation represents very well two of the five dominant observed teleconnection patterns found by WG. A third distinct model pattern (AO) can be viewed as a blend of two observed patterns, which are adjacent to each other in the space domain. The fifth main pattern (Eurasian) known from observations could not be detected in the model data.

3.3. Eigenvector analysis results

The teleconnectivity analysis is essentially a mapping of grid-point correlations. It has a number of shortcomings with respect to pattern recognition: e.g., if two independent patterns interfere in a certain geographical region, a pair of grid-points in this region may display maximum temporal correlation without representing the centres of one distinct variability pattern. Eigenvector (or EOF-) analysis is a more satisfying statistical tool to define variability patterns from a number of centres displaying a highly correlated temporal development. If all teleconnection patterns were completely independent in space and time, then a hemispheric EOF-analysis would yield a sequence of orthogonal principal components (time coefficients) and orthogonal spatial eigenvectors representing the various patterns in the order of their contribution to the total variance. This ideal degree of pattern separation is not found in observational studies, rather the hemispheric eigenvectors tend to show up as combinations of more than one pattern (Horel, 1981). Just the same result was found from the analysis of the simulated patterns (see Table 2 in Subsection 3.4).

To overcome this problem we decided to perform the eigenvector analysis in pre-selected sectors of the hemisphere. The boundaries of the respective sectors were defined according to the spatial extension of the dominant patterns, as they show up in the one-point correlation maps used for the teleconnectivity analysis. A moderate degree of longitudinal overlapping could not be avoided, because we did not want to force an artificial localization of the patterns by a too strict definition of the sector width. In the latitudinal direction the analysis domain was restricted to the area north of 15°N. Thus, all correlation centres appearing on the teleconnectivity map were considered, but most of the tropical belt, where atmospheric interannual variability is directly dominated by SST-variability, was omitted.

The eigenvectors of the first principal component for each of the three chosen sectors are shown in Fig. 3. In all cases the centres of the leading variability patterns are in close coincidence with the correlation centres in Fig. 2. In the Western Pacific sector (Fig. 3a) the first principal component accounts for 35% of the total variance, while the contribution is 27% for the Pacific/North

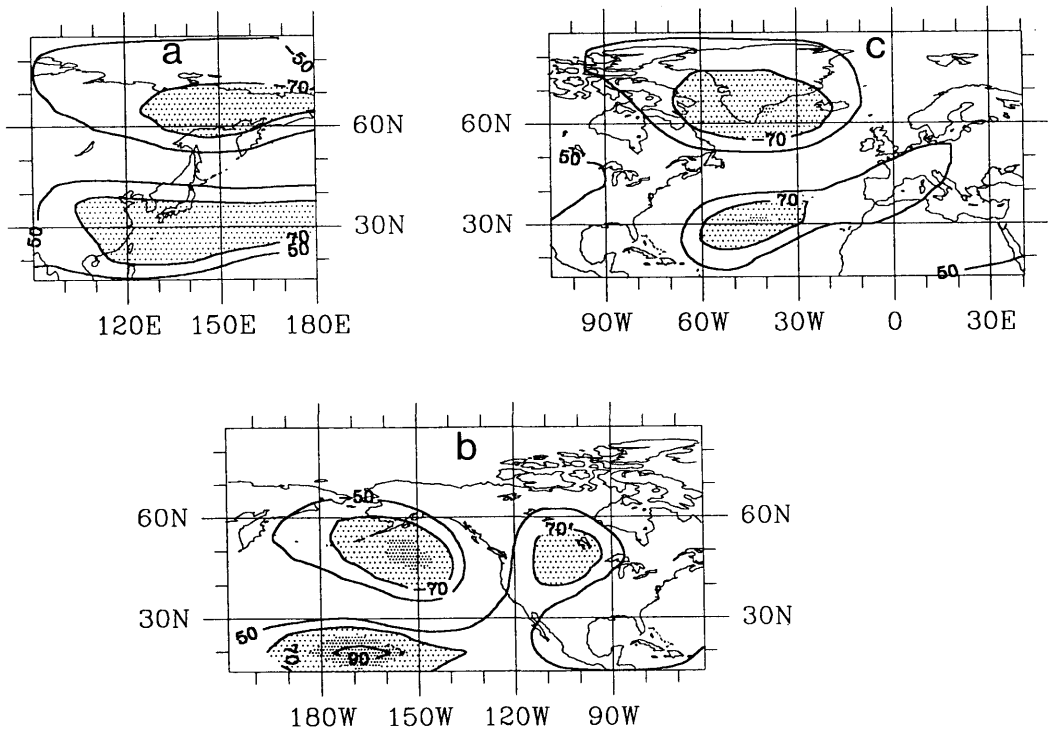


Fig. 3. Leading EOFs of winter-time monthly mean 500 hPa geopotential height data for (a) the West Pacific region (extending from 90° E to 180° W), (b) the Pacific/North American region (from 152° E to 62° W), and (c) the North Atlantic region (from 107° W to 40° E). The units indicate the correlation (in percentage) between the leading principal component and the timeseries of the basic data for each grid point. Light (heavy) shading indicates correlations higher than 70 (85)%.

American sector (Fig. 3b) and 21% for the Atlantic/European sector (Fig. 3c), respectively.

Apart from the consistency between the results of teleconnectivity and EOF-analysis, the simulated patterns are also in general agreement with their observed counterparts. However, the AO pattern is located at least ten degrees to the east of all representatives of WG's WA pattern, as they are found in various observational studies. A possible exception is the January "NAO" structure presented by Barnston and Livezey (1987, their Fig. 2a). The resemblance of various realizations of WG's EA pattern to Fig. 3c is even worse. It should be added that the spatial structure of the second eigenvector for the Atlantic/European sector (not shown) is completely different from both the WA and the EA pattern.

The impression from the teleconnectivity analysis that the American part of the simulated

PNA pattern is not as strongly linked to the Aleutian centre as in the real world is confirmed by the EOF-analysis. The correlation between the first principal component and the timeseries at 30° N, 85° W is less than 0.5 (and thus not recorded in Fig. 3b).

The centres of the WP pattern are similar for teleconnectivity and EOF-analysis. The nature of this pattern as a correlation dipole shows up even more clearly in the structure of the leading eigenvector (Fig. 3a).

3.4. Independence of patterns

It has been established in the preceding sections that the main variability patterns are present in the GAGO integration and that they can be detected by an EOF-analysis as well as by a teleconnectivity analysis. Thus two possibilities are available to represent the time history of the patterns: In the

Table 1. Temporal correlation (for winter months only) of the leading principal component in selected sectors and the related conventional circulation index (after Wallace and Gutzler, 1981)

1st principal component			
Atlantic	PNA	Western Pacific	
0.94	0.55	0.64	AO-index
0.33	0.88	0.21	PNA-index
0.39	0.40	0.90	WP-index

The pattern identifiers for the circulation index definition are the following:

- (1) $\frac{1}{2}[Z^*(30^\circ\text{N}/39^\circ\text{W}) - Z^*(58^\circ\text{N}/39^\circ\text{W})]$ for AO;
 (2) $\frac{1}{4}[Z^*(19^\circ\text{N}/169^\circ\text{W}) - Z^*(47^\circ\text{N}/163^\circ\text{W}) + Z^*(53^\circ\text{N}/107^\circ\text{W}) - Z^*(30^\circ\text{N}/84^\circ\text{W})]$ for PNA;
 (3) $\frac{1}{2}[Z^*(30^\circ\text{N}/146^\circ\text{E}) - Z^*(64^\circ\text{N}/152^\circ\text{E})]$ for WP.

former case the principal components (time coefficients), in the latter case the temporal evolution of circulation indices, as they were introduced by WG. (The pattern identifiers chosen here are given in the caption to Table 1.) The correlation between the principal component and the circulation index timeseries for the same pattern is very high (Table 1), as could be expected from what was presented so far. Both parameters appear appropriate to represent the circulation status in the respected area for a given month.

If the patterns develop quasi-independently in time, as they do in the real world, then the inter-pattern correlation should be weak. Table 2

Table 2. Temporal correlation of the circulation indices for the various circulation patterns (top)

	WP	PNA	AO
AO-index	0.49	0.24	1.00
PNA-index	0.04	1.00	
WP-index	1.00		

	NH	Western Pacific	PNA	Atlantic
Atlantic region	0.86	0.59	0.60	1.00
PNA region	0.77	0.55	1.00	
Western Pacific region	0.86	1.00		
Northern Hemisphere	1.00			

Temporal correlation of the leading principal components associated with the various regional sectors. The correlation with the first hemispheric principal component are given in the first column (bottom).

shows the temporal correlation between the three conventional circulation indices (a), and the three leading principal components (b). The result remains equivocal.

The weak correlation of the PNA-index with both the AO- and the WP-index indeed suggests a definite independence. However, the correlation between the principal components appears to be artificially enhanced as a consequence of the overlapping between the spatial domains used for the EOF-analysis. A moderate degree of temporal correlation between the AO and the WP pattern seems to be actual in the model framework, a relation that has not been reported in observational studies.

4. The influence of variable SST forcing

It is plain from observational as well as from GCM studies that only a small part of interannual extratropical geopotential height variance can be attributed to interannual variability of tropical or extratropical SST forcing. It has proved not easy to establish well-defined, significant response patterns of the extratropical atmosphere to anomalous SST conditions on the basis of observational data. Even more difficult to solve is the problem of separating the influence of tropical and extratropical SST anomalies to the total response for a particular situation.

If the problem to determine the influence of SST variability on the extratropical atmospheric variability is approached on the basis of GCM simulations (a recent review of respective experiments has been given by Lau, 1993), the main advantage over observational studies is the possibility to switch on and off the SST forcing at will, either on the global scale or even in certain geographical regions. Thus one can hope to isolate particular SST forcing effects from the variety of cause and effect relationships, given that the model offers a reasonable description of the real world.

Having established the existence of realistic variability patterns in the GAGO run in the previous section it is worth considering the results from a second long-range integration (the CONTROL run) with completely the same model, but with interannual variability of SST switched off. The effect of this change is most significant in the tropics, where the interannual

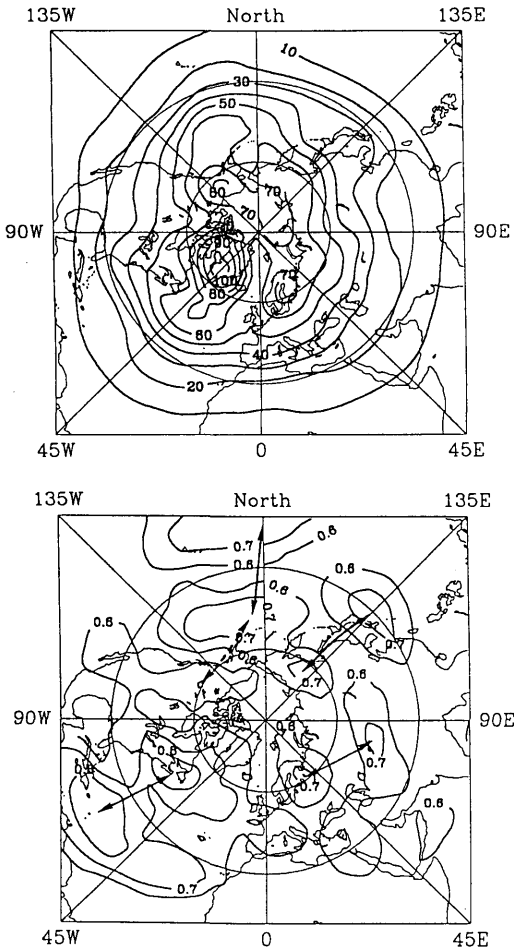


Fig. 4. Top panel shows the interannual standard deviation of winter-time monthly mean 500 hPa geopotential height data for the CONTROL integration. Bottom panel shows the teleconnectivity map for the CONTROL integration (to be compared with Fig. 2 for the GAGO integration).

variance of atmospheric parameters like temperature, geopotential height or precipitation in the GAGO run ranges 10 to 20 times larger than in the CONTROL run (not shown). However, in close agreement with results reported by Palmer (1987, his Fig. 11) very few extratropical regions exhibit an enhancement of variance in the GAGO run that can be assessed as significant. The overall level of interannual extratropical variability is dominated by internal atmospheric processes.

In view of the apparently insignificant effect of

year-to-year SST variation to the extratropical interannual variance the result of a comparison of the respective teleconnectivity maps may look surprising. The PNA pattern, for example, is rather obscure in the CONTROL run (Fig. 4). Its centres are less strongly correlated and particularly the Canadian maximum is hardly recognizable as a distinct feature. In the North Atlantic sector the differences are most striking: The dipole pattern in the GAGO run (Fig. 2) that could be interpreted as a counterpart of the observed AO, is shifted 20° westward and 15° southward in the CONTROL run. This implies that the northern correlation centre (over Newfoundland) has moved away from the region of maximum variability, which is located over southern Greenland in both integrations.

The WP pattern is the only one, which is little different in the GAGO and the CONTROL run. While a considerable degree of correlation between the WP index and an index representing the temporal behaviour of (tropical and extratropical) Pacific SSTs was found by Horel and Wallace (1981), the more recent work of Wallace et al. (1990) does not support the conclusion that those correlations arise from SST forcing of the atmosphere. Rather, the WP pattern appears as an important mode with respect to atmospheric forcing of the extratropical ocean. Hence, our results concerning this pattern are in accordance with the expectations.

It is evident that including the forcing effect of interannual SST variability on a global scale, though it does not significantly enhance the level of extratropical atmospheric variance, helps to simulate more realistic atmospheric correlation patterns. Lau and Nath (1990) used a simulation similar to ours for a diagnostic study of the related causes and effects, in particular with respect to the competing influence of tropical and extratropical SST forcing. However, due to the complexity of this problem a thorough discussion is regarded to be beyond the scope of the present paper. We return to this point in the concluding section.

5. Pattern transitions and transient variability

5.1. Motivation and procedure

The modes of variability discussed in the previous sections have the character of large-scale

circulation regimes, which may be excited with one sign or the other for a given month. The time history is reflected by the principal components or the temporal evolution of the circulation indices, respectively. In this section the sensitivity of certain regional climate features to circulation regime transitions will be discussed. Such an attempt can be, on one hand, regarded as a more sophisticated step of model validation. Another point is that the changes of regional climate conditions simulated in a response experiment can be accepted with more confidence, if the variability in the respective region is related to large scale pattern fluctuations (Von Storch et al., 1993). The latter are in many respects realistically and consistently represented by the ECHAM model, as has been shown above, while a localized small scale response must be a priori interpreted with caution.

Our consideration of regional climate variability will mainly be based on the fundamental elements of intraseasonal transient variability, i.e., cyclones and quasi-stationary persistent anomalies of either sign. There are two different approaches to this matter. Either individual synoptic events can be counted for each grid point or the spatial distribution of the temporal standard deviation can be determined for the time scales involved. Certainly the former method is most straightforward and it offers the possibility to consider the synoptic development of each selected event. The second method allows a simple statistical estimation of variability and interactions. However, its main advantage is a clear-cut separation of the different time scales. The second method has been used more commonly for both observed and simulated data and a rich treasure of comparable results has been accumulated since the pioneering work of Blackmon (1976).

For a most suggestive characterisation of the circulation regimes established in Section 3 we will use a combined presentation of both possible methods to determine transient variability. The way of cyclone identification is adopted from König et al. (1993). It has been developed on the basis of characteristic features of the 1000 hPa geopotential height and the 850 hPa vorticity fields. The identification routine for quasi-stationary circulation systems ("blocking") is briefly described in the Appendix.

Composites for each regime are constructed in the following way: First, the total of 57 monthly

means is partitioned into sub-ensembles that are associated with an extreme (positive or negative) value of one of the circulation indices. Second, appropriate circulation parameters are sampled over the sub-ensembles. For example, the characteristic storm track structure belonging to a circulation regime is reflected by the maxima of cyclone frequency (König et al., 1993) or by the largest values of bandpass-filtered daily geopotential height variability (Blackmon, 1976) for the respective sub-ensemble. It is clear that this approach is not designed to capture the cause and effect relationship between mean flow and various transients during regime transitions. We are simply estimating the statistical stationary response of the local eddy activity arising from changes of a variability pattern from one mode to the other.

5.2. Results

The time series of the PNA circulation index is shown in Fig. 5a. Positive values indicate a deepening of the Aleutian trough with respect to its climatological strength. "Extreme" positive or negative pattern polarity is defined to exist for a certain month, if the index is larger than half of the temporal standard deviation. This yields two composites consisting of either 18 months with strong positive index or 15 months with strong negative index. (The remaining months do not enter the ensemble statistics.) The difference of the 500 hPa monthly mean geopotential height distributions between the "+PNA" and the "-PNA" sub-ensembles is displayed in Fig. 5b. By construction, the result must be a distinct image of the PNA pattern whose centers have been used to define the index.

To illustrate the storm track shapes associated with "+PNA" and "-PNA" events a combination of cyclone frequency rate and bandpass-filtered 500 hPa geopotential height variability is presented in Fig. 6. As usual, the eddy variability is represented by contour lines of equal standard deviation, while we use dots of varying size to display the cyclone-frequency at each grid point. Evidently, the storm track axes suggested by both methods do not coincide. The surface cyclones appear to follow a path northward of the maximum bandpass-filtered height variance. A smaller part of the difference may be attributed to different positions of cyclone centres in the lower and middle troposphere. However, the main reason is

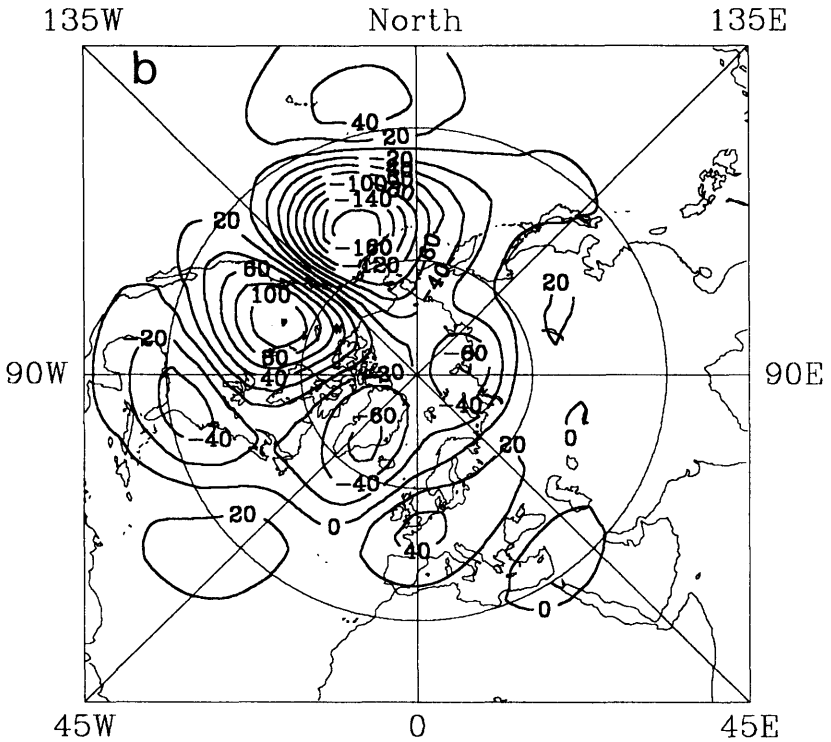
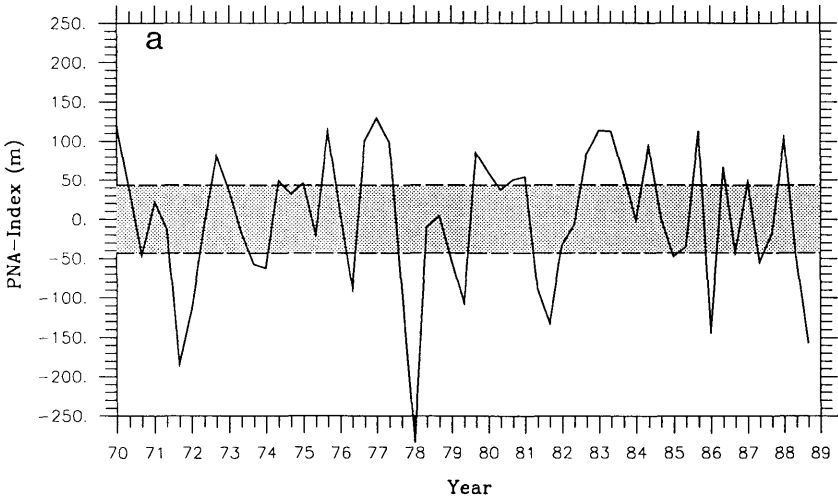


Fig. 5. (a) Timeseries of the PNA circulation index for the GAGO run. Only the January, February and December months are considered for each year. Shaded area denotes a band of 0.5 of the temporal standard deviation of the index values. (b) Difference of 500 hPa geopotential height mean between positive and negative PNA-events (units: gpm).

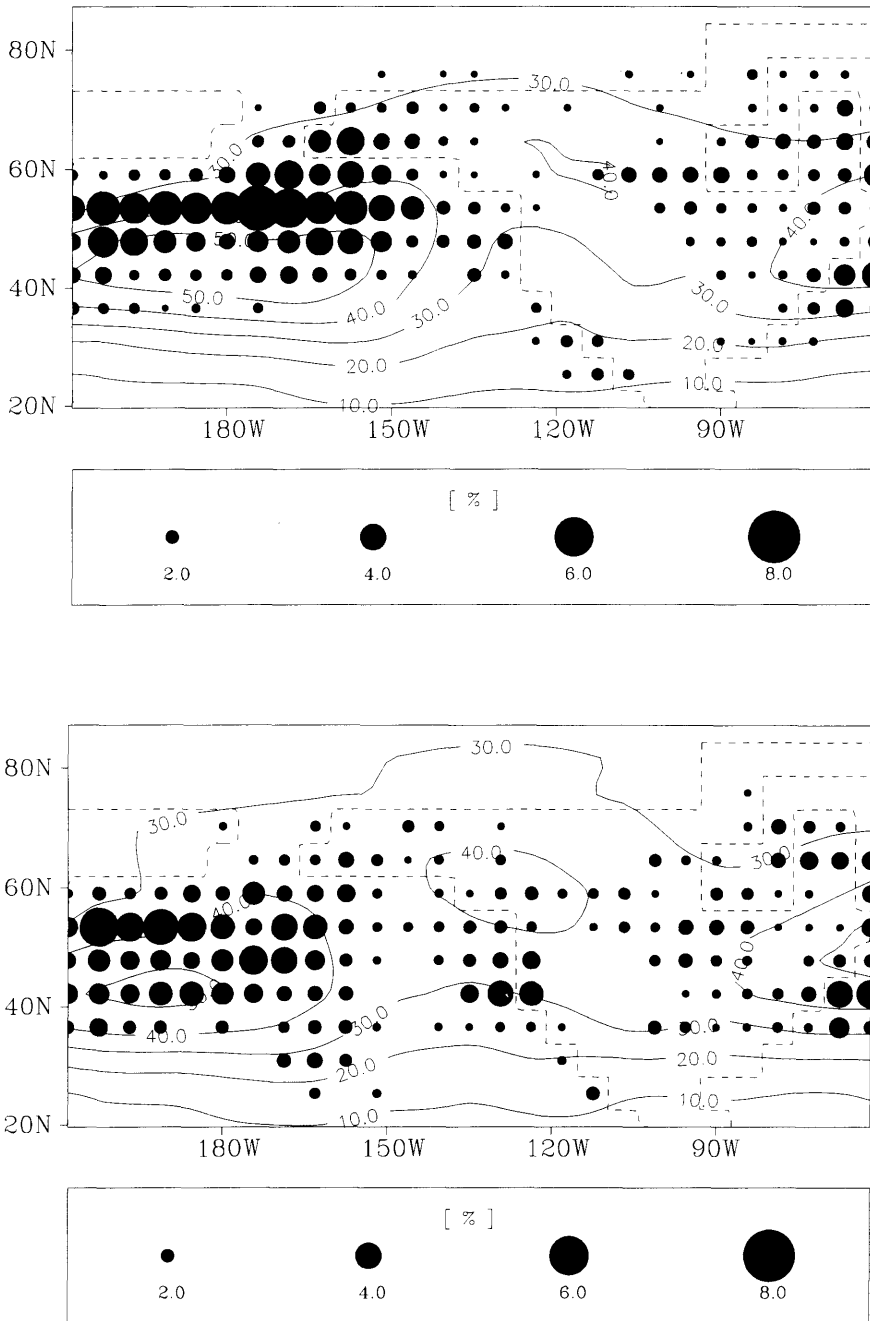


Fig. 6. Top panel shows mean cyclone frequency over the North Pacific and North America for all months with "extreme" positive PNA-index (cf. Fig. 5a). The area of a circle is proportional to the cyclone frequency (i.e., number of occurrences of a cyclone at each gridpoint, in percentage of the total of days). Contour lines represent standard deviation of filtered geopotential height at 500 hPa (units gpm). Bottom panel gives the equivalent for cases with "extreme" negative PNA-index.

given by the underlying zonal mean pressure gradient that causes the cyclone (anticyclone) centres to be shifted to the north (south) with respect to latitude of maximum anomaly (Wallace et al., 1988). In Fig. 6 the northward shift predominates, as we consider synoptic cyclones only.

Despite the difference in positioning the climatological mean storm track axis, its displacement from the “+PNA” to the “-PNA” regime shows up consistently for both methods. The strengthening of the Aleutian low in the case of “+PNA” events (Fig. 5b) is accompanied by enhancement of cyclonic activity in the eastern Pacific between 40°N and 60°N (Fig. 6a). The differences of the bandpass-filtered height variability is in nice accordance with similar results derived from observations by Lau (1988). Though Lau used a different procedure to yield his patterns, his “P2” regime has essentially the same mean flow characteristics as our PNA pattern. As he points out (Lau, 1988, his Figs. 6c, d) the positive PNA mode is associated with enhanced bandpass-filtered variance to the east of the dateline, just as in our model (Fig. 6a). On the other hand, according to Lau’s results the storm track should be found deflected to the north with enhanced activity over the Gulf of Alaska for the negative PNA mode. The model shows rather a weakening of cyclonic activity all over the eastern North Pacific with only a slight hint of variability enhancement over northwestern Canada. However, an increase of cyclone frequency around the coast of Washington and Oregon is indicated (Fig. 6b).

The hemispheric distribution of low-frequency variability, for positive and negative PNA mode respectively, is displayed in Fig. 7 by means of the standard deviation of 5-day 500 hPa geopotential height means belonging to either mode. The substantial enhancement of 5-day mean variability that is found for the negative PNA events is in remarkable agreement with observational evidence presented by Palmer (1988, his Figs. 12d, e). Considering results of a barotropic model Palmer argues that the negative PNA-mode might be a circulation state of higher barotropic instability and thus enhanced internal low-frequency variability. It appears that the ECHAM model simulates the barotropic stability characteristics of the observed atmosphere in the Pacific/North American region well. The variability of 500 hPa geopotential height on time scales larger than about seven days

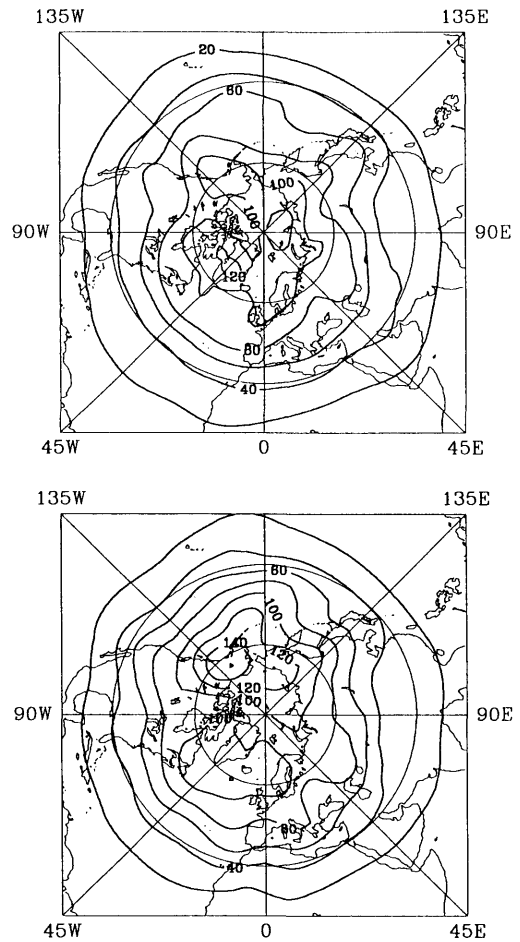


Fig. 7. Standard deviation of 5-day means of 500 hPa geopotential height data (units: gpm) for the months with “extreme” positive PNA-events (top) and for the months with “extreme” negative PNA-events (bottom).

is known to be closely related to a more or less frequent occurrence of persistent circulation anomalies. As demonstrated by Blackmon et al. (1986), the maxima of lowpass-filtered height variance define the preferred location of both positive and negative geopotential anomalies. Positive anomalies (blocking) are somewhat more frequent than negative ones. The standard deviations in Fig. 7 were calculated independently for the “+PNA” and “-PNA” sample, i.e., with respect to different ensemble means. Thus we have to make sure that the enhancement of intraseasonal low-frequency variability for the

“-PNA” case is indeed accompanied by a larger number of persistent anomalies with respect to the climatological mean. This is demonstrated in Fig. 8, where positive and negative persistent anomalies are considered separately. While nearly no anomalies are found in the “+PNA” ensemble, they occur frequently in the opposite case. There are, in particular, many blocking events near the North Pacific centre of the PNA pattern (where the Aleutian low is weaker than normal). Most of the negative anomalies develop further eastward, over western Canada.

An analogous classification procedure for the

North Atlantic region yields 19 samples of strong positive AO-index (which, in contrast to WG's definition, indicates anomalously low pressure to the south of Greenland) and 17 samples with strong negative index (Fig. 9a). The related composites of the bandpass-filtered standard deviation and of the cyclone frequency are displayed in Fig. 10. Again a comparison with the observational results reported by Lau (1988) for the same region is tempting. Lau finds that the fluctuations of the WA pattern (as defined by WG) are associated with a strengthening or weakening of cyclonic activity in the cyclogenesis region off the

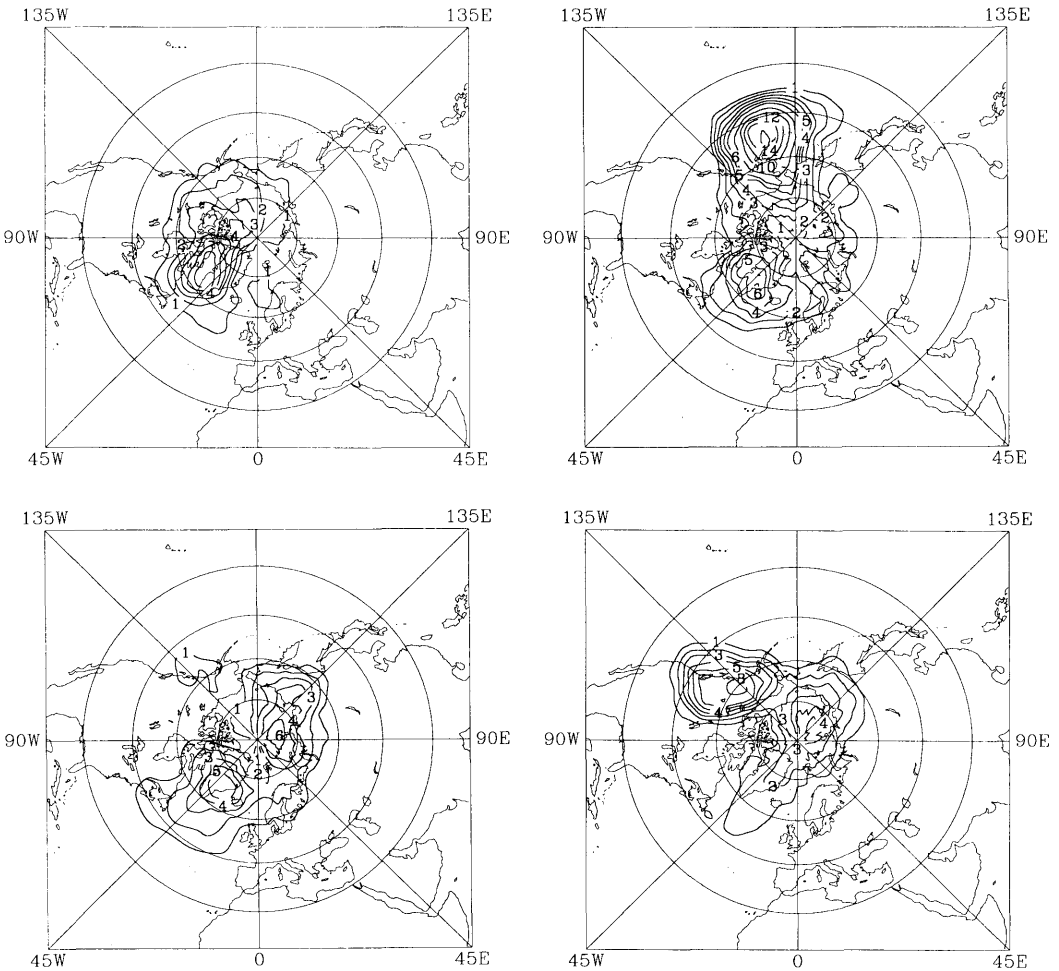


Fig. 8. Frequency of persistent anomalies (percentage of the total of days) in geopotential height field at 500 hPa in the Northern Hemisphere. Upper panels: positive anomalies (blocking), lower panels: negative anomalies (cut-off lows). Left: for months with “extreme” positive PNA-index. Right: for months with “extreme” negative PNA-index.

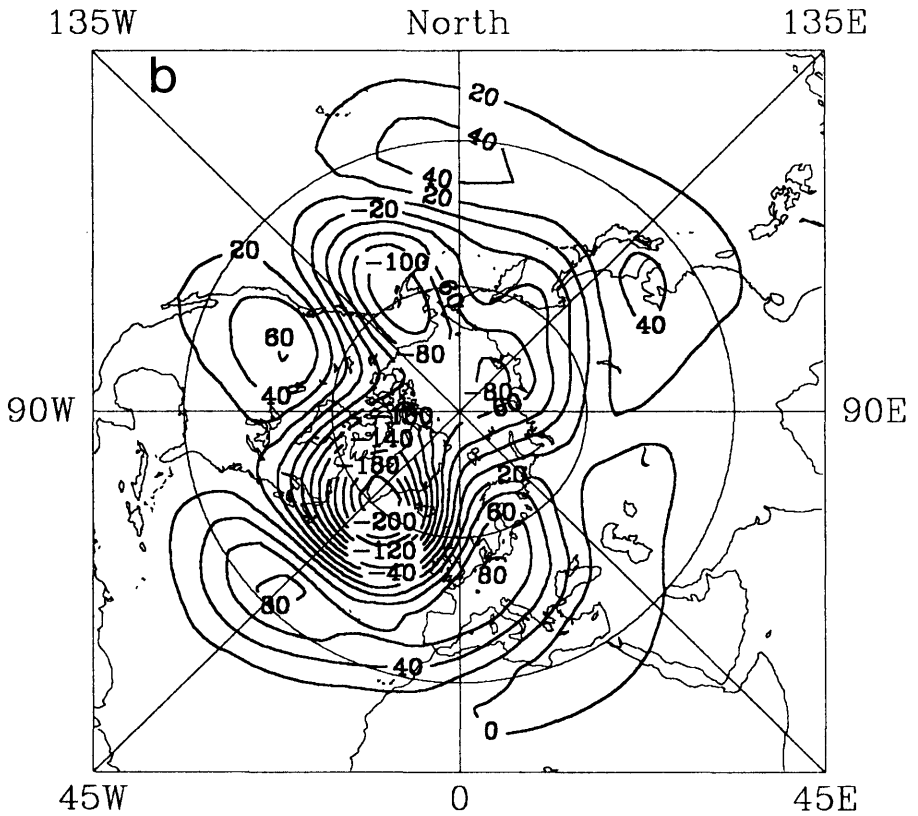
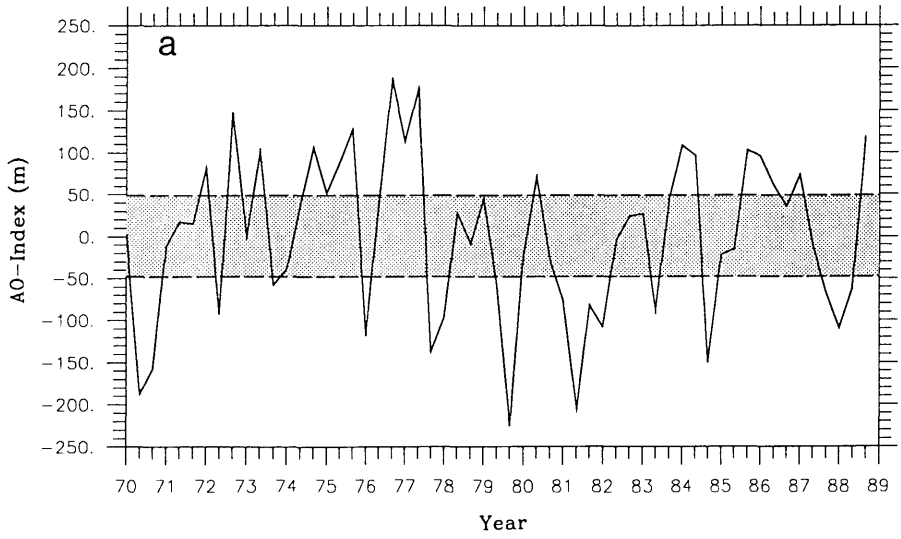


Fig. 9. As Fig. 5, but with respect to the AO circulation index.

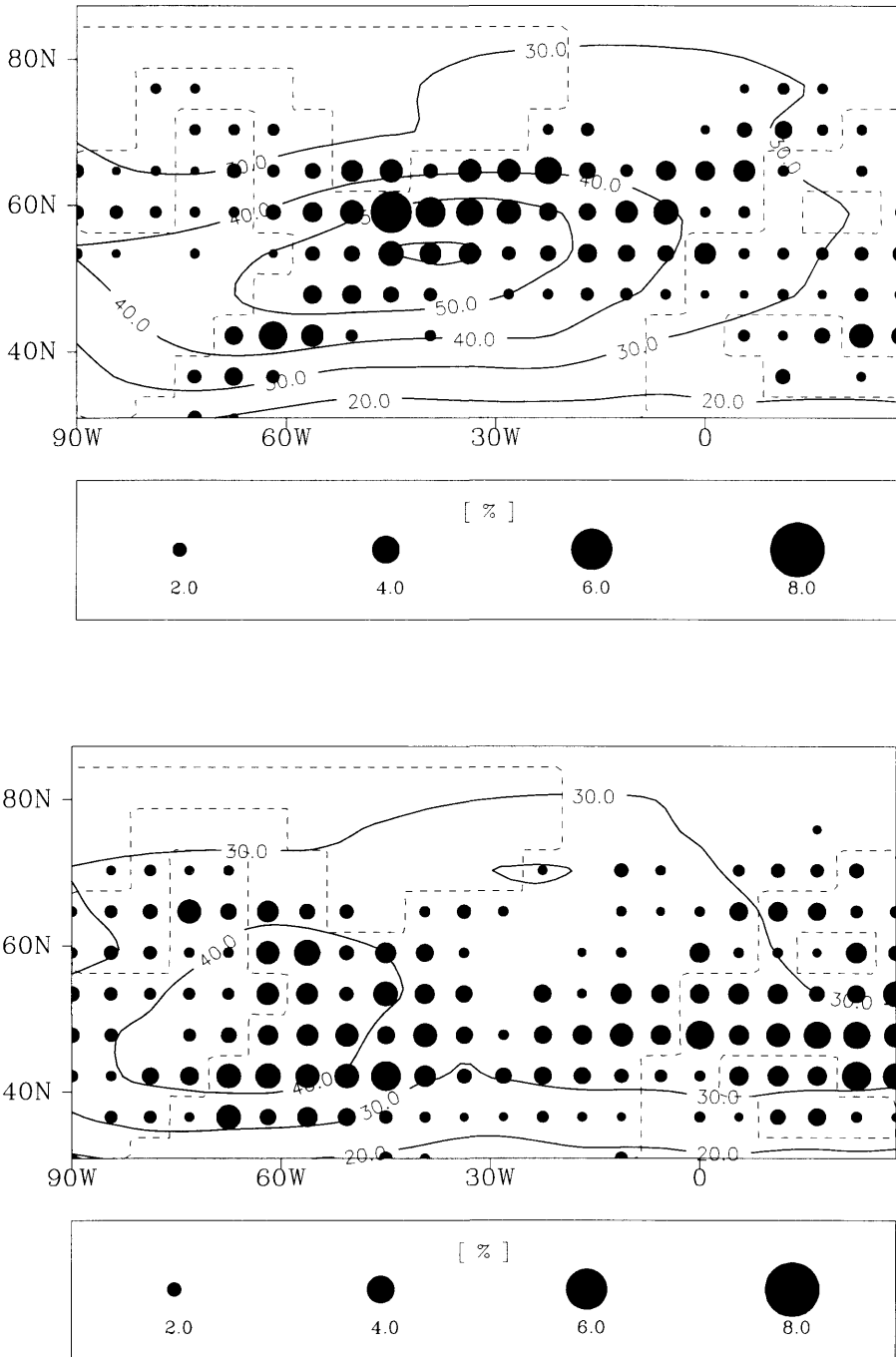


Fig. 10. Top panel shows mean cyclone frequency over the North Atlantic for all months with "extreme" positive AO-index (cf. Fig. 9). For legends cf. Fig. 6. Bottom panel gives the equivalent for the cases with "extreme" negative AO-index.

east coast of North America (“A1-mode”, Lau, 1988, his Fig. 7c). The modes of WG’s EA Pattern determine the structure of the storm track at its eastern part (Lau’s “A2-mode”). If there is a negative height anomaly in the central Atlantic (and the Icelandic low is deeper than normal) the cyclones are steered towards the Iberian peninsula. In the opposite mode the storm track is deflected towards the Icelandic region. In the model simulation AO (Fig. 2, Fig. 3c, Fig. 9b) substitutes both the observed WA and EA patterns. Consequently the AO-related storm track modes appear as a blend of the respective observational structures, too. Strong cyclonic activity along the climatologi-

cal storm track axis, as it goes with the “+AO”-mode (Fig. 10a), mainly reminds of the “high A2” mode of Lau (1988). The diffuse and rather weakly developed storm track associated with “-AO” (Fig. 10b) can be regarded as a compromise of the “low A1” and “low A2” modes of Lau (1988, his Figs. 7b, d). Similar to the “-PNA”-case, the distinct storm track deflection to the northeast observed for cases of an anomalously weak Icelandic low (Lau’s “low A1”-mode) is hardly indicated by the model. Enhanced cyclone activity over Southern Europe in the “-AO” ensemble (Fig. 10b) is not evident from Lau’s observational results. The climatological bandpass-filtered eddy

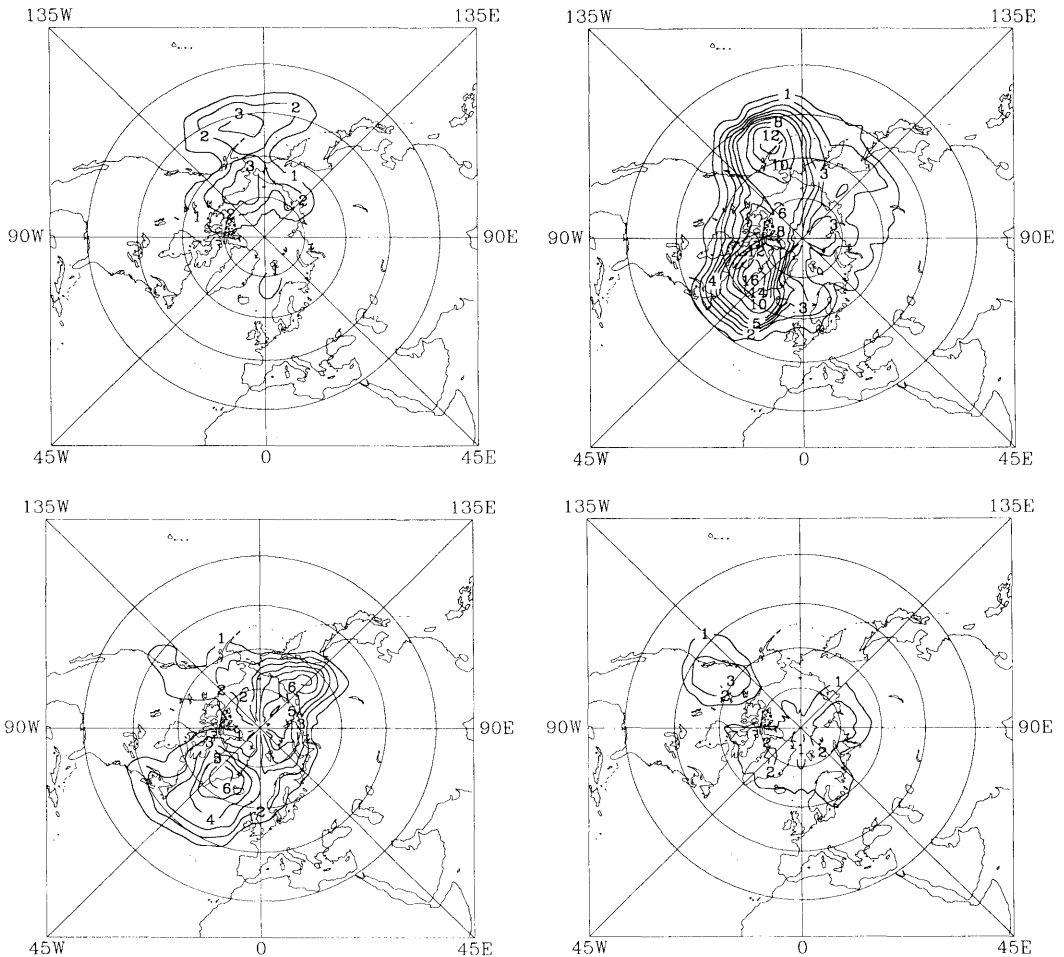


Fig. 11. As Fig. 8, but for months associated with positive AO-index (left panels) and negative AO-index (right panels).

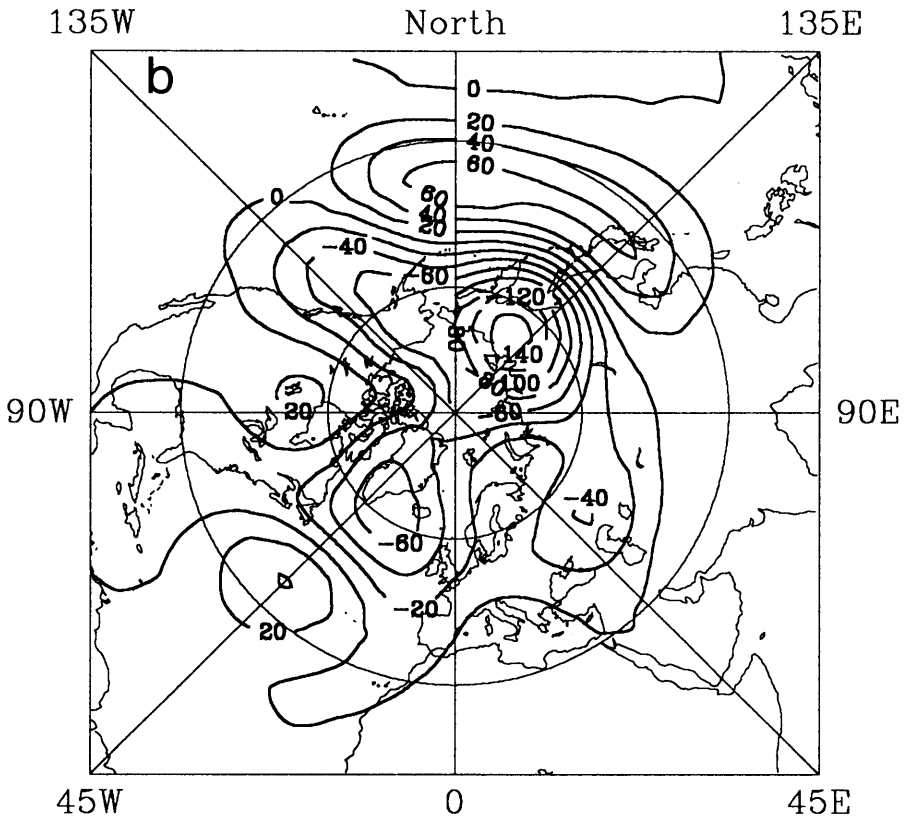
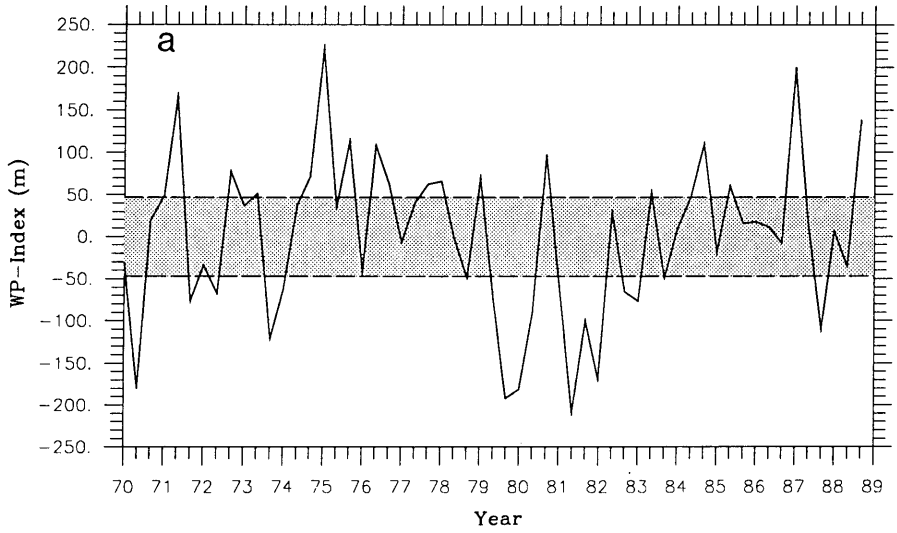


Fig. 12. As Fig. 5, but with respect to the WP circulation index.

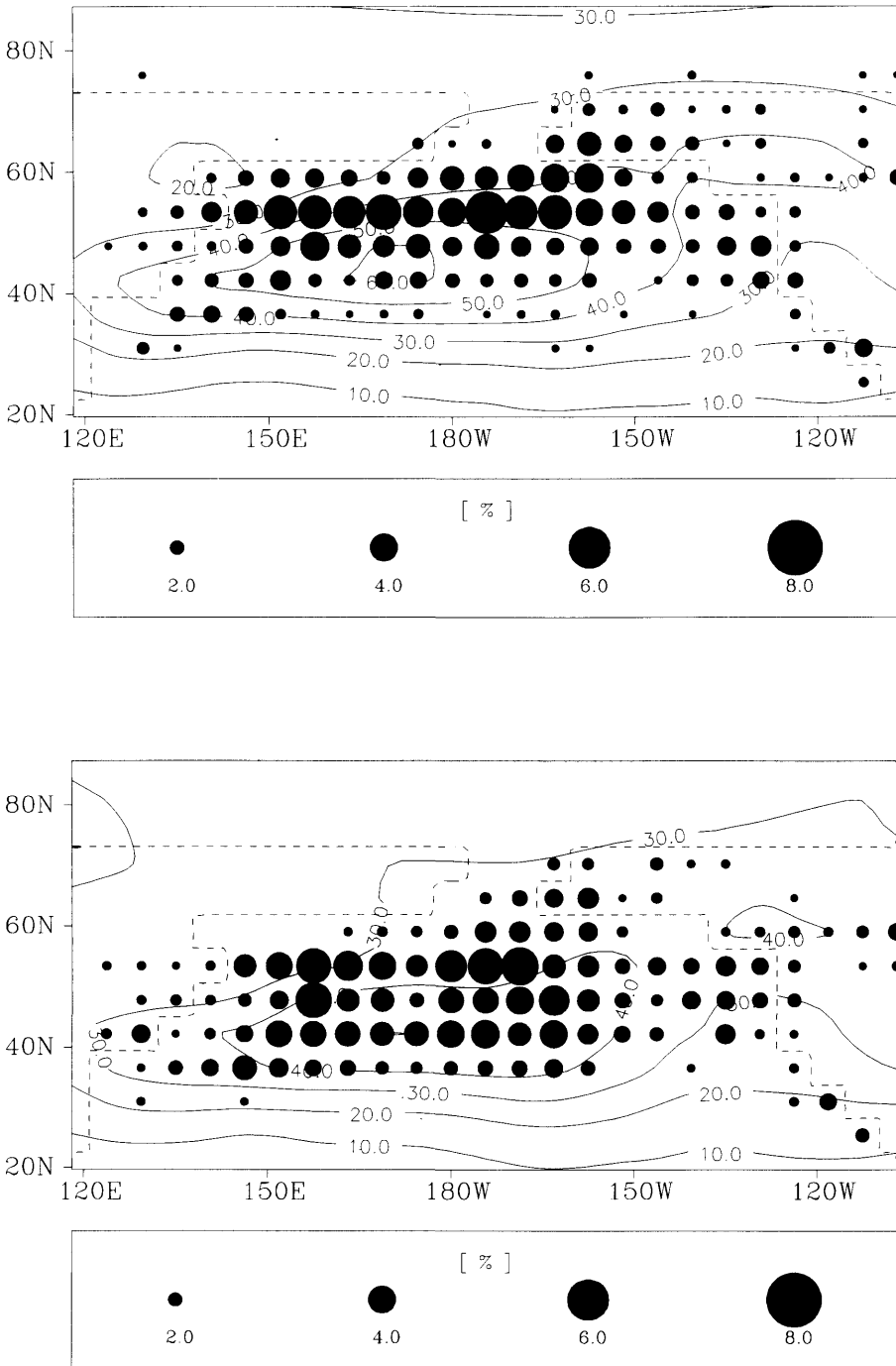


Fig. 13. As Fig. 6, but for months associated with positive (top) and negative (bottom) WP-index, as determined according to Fig. 12.

variance over Europe is much weaker than over the Atlantic, and related fluctuations may have failed to find entrance in Lau's analysis of this quantity. The variability of 5-day means is very similar for both modes of AO, thus the respective figures are omitted here. A strong difference with respect to the formation of circulation anomalies shows up, however (Fig. 11). In the "–AO" case, where the Icelandic low is weak, blocking is a frequent phenomenon in the North Atlantic and negative anomalies occur quite rarely. If the Icelandic low is stronger than normal, there is a tendency towards the formation of negative anomalies in the same region, while blocking almost never occurs (Fig. 11, left panels).

For the modes of the West Pacific pattern we find 18 events with strong positive WP-index (indicating a strengthened trough over Siberia) and 17 events with strong negative index (Fig. 12). The bandpass-filtered transient eddy variability (Fig. 13) is uniformly enhanced to the west of the dateline in the "+WP"-mode. The strongest increase occurs around 45°N, 170°E. In some contrast to this monopole-like response the cyclone frequency exhibits a northward shift for the "+WP"-composite, while cyclone migration along 40°N appears to be more frequent for negative pattern polarity. A similar shift is found for the Pacific jet stream between 150°E and the dateline (not shown). To the east of the dateline differences between the composites can be found, too, but they are much weaker than those discussed for the modes of the PNA pattern (Fig. 6). The storm track response to be noticed in Fig. 13 reminds strongly of the characteristics of the "P1"-mode by Lau (1988). Actually Lau considers his "P1"-mode to be associated with the WP pattern. The respective mean flow response, however, appears to be somewhat different in the observed atmosphere (Fig. 11a of Lau, 1988) and in the simulation (Fig. 12a). No significant impact of the west Pacific pattern modes to intraseasonal low-frequency variability could be found.

6. Discussion

We have used a number of diagnostic tools to establish the existence of interannual variability

patterns, as well as the relation of these patterns to intraseasonal transient activity, in a circulation model of low horizontal resolution.

The simulation of the interannual variability component is very satisfactory. The level of variance and the structure of the leading patterns (Fig. 2) are both captured. The reasonable performance of the ECHAM2/T21 GCM must be fully appreciated, because it has been suggested that low-resolution models produce a realistic simulation of the Northern Hemisphere time-mean state mainly due to a compensation of errors (Palmer, 1987). Despite the resolution-dependent drawbacks of a T21 GCM, that have often been addressed, a realistic simulation of the space/time structure of extratropical interannual variability can be achieved. In this respect the efforts to improve the physical parameterizations have borne fruits.

The relation of local transient activity to the variability modes of the monthly mean flow (Section 5) is in good agreement with observational evidence, a fact of great importance for the use of the model as a climate prediction tool. The simulation of extratropical variability on a variety of time scales from the cyclonic up to the interannual yields a self-consistent and fairly realistic image of reality. We conclude that the model offers considerable prospects for deducing various local climate changes from the large-scale response (e.g., along the path sketched by Von Storch et al., 1992).

Nevertheless, systematic deficiencies of the model still show up for particular situations. For example, the problems of low resolution models in simulating the cyclone-scale forcing on the larger scales seem to culminate in the later stages of the baroclinic life cycle. Metz and Lu (1990) and Ponater et al. (1990) have shown results to support this view for the T21-model (though they used a version previous to the one discussed here). These problems are likely responsible for the model's failure to simulate the observed deflection of cyclone migration to the northeast in the "–AO"- and "–PNA"-cases. More detailed diagnosis including transient eddy transports or Eliassen-Palm-flux statistics might help to understand the systematic errors of a deficient scale interaction more clearly. Even with such knowledge at hand, however, the crucial question, whether the systematic errors in the cyclone-scale

forcing deteriorate the mean flow simulation, or whether the erroneous characteristics of the mean flow (e.g., the absence of a clear-cut EA pattern) dominate the storm track structure, would remain difficult to answer.

It has been pointed out in Section 4 that the inclusion of interannual sea surface temperature variation as a boundary forcing is essential for a realistic simulation of the patterns of extratropical interannual variability. A discussion of the cause and effect relationships basic to this fact is beyond the scope of this paper. The SST field and its variability were prescribed on a global scale, thus a separation of the combined effect of tropical and extratropical forcing is hardly possible. However, this problem will be approached in a subsequent paper (Graham et al., 1994) on the basis of additional simulations, in which the SST forcing will be restricted to either tropical or extratropical regions.

7. Acknowledgements

We gratefully appreciate the assistance of Dipl.-Met. Reinhard Voß and Dipl.-Oc. Marina Candouna in creating part of the software required for this study. We also thank Dr. Ute Luksch and Dr. Werner Metz for valuable discussions during the developing phase of our work. In using the designation "Atlantic Oscillation" for the leading pattern in the Atlantic region we adopted the suggestion of an unknown reviewer. The ECMWF observational data were used by permission of the German Weather Service. This work has been supported by the Bundesminister für Forschung und Technologie (07 KFT 05/6) and by the Deutsche Forschungsgemeinschaft (SFB 318).

8. Appendix

An objective blocking index based on a synoptical point of view

For an appropriate blocking statistics not only the frequency of extreme positive anomalies in the geopotential height field has to be considered, but also the duration and the spatial correlation of these anomalies should be taken into account. While the spatial distribution of lowpass-filtered height variance can be used for identifying regions of high blocking frequency (Blackmon et al., 1986), this method does not distinguish between positive and negative anomalies. Using a pre-defined longitudinal extent of the anomalies as a selection criterion is also possible (Lejenäs and Økland, 1983).

In the present paper we have chosen a method closer to the synoptician's way of defining blocking events: An anomaly $Z'(\lambda, \varphi, t)$ of the 500 hPa geopotential height is calculated by removing the annual mean, the mean annual cycle and a 30-day running mean from the basic time series. In order to filter out the blocking events from the three-dimensional (λ, φ, t) -space, we search for contiguous areas with $Z' \geq 300$ gpm that exist for at least five days. The detected areas are extended to those contiguous points of the (λ, φ, t) -space that show up an anomaly of $Z' \geq 250$ gpm. This way of proceeding takes into account the fact that a block is usually not located at a fixed position for its whole lifetime, but may move both zonally and meridionally. The results are not very sensitive to the threshold value of five days for the duration of the mature phase.

Negative anomalies (i.e., cut-off lows) can be detected in a completely analogous way by using anomaly thresholds of -300 hPa and -250 hPa, respectively. A detailed description of the method and its validation is given by Sausen et al. (1993).

REFERENCES

- Barnett, T. P., Latif, M., Kirk, E. and Roeckner, E. 1991. On ENSO physics. *J. Clim.* **4**, 487–515.
- Barnston, A. and Livezey, E. 1987. Classification, seasonality and persistence of low-frequency circulation patterns. *Mon. Wea. Rev.* **115**, 1083–1126.
- Blackmon, M. L. 1976. A climatological spectral study of the 500 mb geopotential height of the Northern Hemisphere. *J. Atmos. Sci.* **33**, 1607–1623.
- Blackmon, M. L., Mullen, S. L. and Bates, G. T. 1986. The Climatology of blocking events in a perpetual January simulation of a spectral general circulation model. *J. Atmos. Sci.* **43**, 1379–1405.
- Cubasch, U., Hasselmann, K., Höck, H., Maier-Reimer, E., Mikolajewicz, U., Santer, B. D. and Sausen, R. 1992. Time-dependent greenhouse warming computations with a coupled ocean-atmosphere model. *Climate Dynamics* **8**, 55–69.
- Esbensen, S. K. 1984. A comparison of intermonthly and

- interannual teleconnections in the 700 mb geopotential height field in the Northern Hemisphere winter. *J. Atmos. Sci.* **112**, 2016–2032.
- Fischer, G. (Ed.), 1989. Climate simulations with the ECMWF T21-model in Hamburg. *Meteorologisches Institut der Universität Hamburg, Report No. 1*, 159 pp.
- Fischer, G. (Ed.), 1989. Climate simulations with the ECMWF T21-model in Hamburg. Part III: Diagnosis of response experiments. *Meteorologisches Institut der Universität Hamburg, Report No. 7*, 247 pp.
- Graham, N. E., Ponater, M., Barnett, T. P., Wilde, R. and Schubert, S. 1994. On the roles of tropical and mid-latitude SSTs in forcing interannual to interdecadal variability in the winter Northern Hemisphere circulation. *J. Clim.* **6**, in press.
- Horel, J. D. 1981. A rotated principal component analysis of the interannual variability of the Northern Hemisphere 500 mb height field. *Mon. Wea. Rev.* **109**, 2080–2092.
- Horel, J. D. and Wallace, J. M. 1981. Planetary-scale atmospheric phenomena associated with the Southern Oscillation. *Mon. Wea. Rev.* **109**, 813–829.
- König, W., Sausen, R. and Sielmann, F. 1993. Objective identification of cyclones in GCM simulations. *J. Clim.* **6**, 2217–2231.
- Kushnir, Y. and Wallace, J. M. 1989. Low-frequency variability in the Northern Hemisphere winter: Geographical distribution, structure and time-scale dependence. *J. Atmos. Sci.* **46**, 3122–3142.
- Lau, N.-C. 1988. Variability of the observed mid-latitude storm tracks in relation to low-frequency changes of the circulation pattern. *J. Atmos. Sci.* **45**, 2718–2743.
- Lau, N.-C. 1993. Climate variability simulated in GCMs. In: *Climate system modeling*, (ed. K. Trenberth), Cambridge University Press, 617–643.
- Lau, N.-C. and Nath, M. J. 1990. A general circulation model study of the atmospheric response to extratropical SST anomalies observed in 1950–79. *J. Clim.* **3**, 965–989.
- Lejenäs, H. and Økland, H. 1983. Characteristics of northern hemisphere blocking as determined from a long time series of observation data. *Tellus* **35A**, 350–362.
- Metz, W. and Lu, M.-M. 1990. Storm track eddies in the atmosphere and in an ECMWF T21 climate model. *Beitr. Phys. Atmos.* **63**, 25–40.
- Palmer, T. N. 1987. Modelling low-frequency variability of the atmosphere. In: *Atmospheric and oceanic variability* (ed. H. Cattle). Royal Meteorological Society, 75–103.
- Palmer, T. N. 1989. Medium and extended range predictability and stability of the Pacific/North American mode. *Q. J. R. Meteorol. Soc.* **114**, 691–713.
- Ponater, M., Kirk, E. and Schlese, U. 1990. GCM-simulated transient variability in the Northern Hemisphere extratropics and its sensitivity to sea surface temperature variation. *Beitr. Phys. Atmos.* **63**, 189–204.
- Roeckner, E., Arpe, K., Brinkop, S., Dümenil, L., Esch, M., Kirk, E., Lunkeit, F., Ponater, M., Rockel, B., Sausen, R., Schlese, U., Schubert, S. and Windelband, M. 1992. Simulation of the present-day climate with the ECHAM model: Impact of model physics and resolution. *Max-Planck-Institut für Meteorologie, Report No. 93*, 171 pp.
- Sausen, R., König, W. and Sielmann, F. 1993. Analysis of blocking events from observations and ECHAM model simulations. *Meteorologisches Institut der Universität Hamburg, Report No. 11*, 30 pp.
- von Storch, H., Zorita, E. and Cubasch, U. 1992. Down-scaling of global climate change estimates to regional scales: An application to Iberian rainfall in wintertime. *J. Clim.* **6**, 1161–1171.
- Walker, G. T. and Bliss, E. W. 1932. World Weather V. *Mem. Roy. Meteor. Soc.* **4**, 53–84.
- Wallace, J. M. and Blackmon, M. L. 1983. Observations of low-frequency atmospheric variability. In: *Large-scale dynamical processes in the atmosphere* (eds. B. Hoskins and R. Pearce). Academic Press, 55–94.
- Wallace, J. M. and Gutzler, D. S. 1981. Teleconnections in the geopotential height field during the Northern Hemisphere winter. *Mon. Wea. Rev.* **106**, 296–310.
- Wallace, J. M., Lim, G.-H. and Blackmon, M. L. 1988. Relationship between cyclone tracks, anticyclone tracks and baroclinic wave guides. *J. Atmos. Sci.* **45**, 439–462.
- Wallace, J. M., Smith, C. and Jiang Quanrong, 1990. Spatial patterns of atmosphere-ocean interactions in northern winter. *J. Clim.* **3**, 990–998.